energy and subsequent earlier formation of the capillary waves leads to an earlier receding and retraction of the cavity, seen clearly in Figure 5.31(a) for all wave angles.

In Figure 5.31(b) the time evolutions of the depths of the cavities upon impingement onto different phases of the large amplified wave are presented for both liquids. The clear differences between both liquids, found for the impingement onto steady liquid films and small solitary waves, are not observed here. The rate of leveling of the curves, the value of the maximum depth of the cavity and the time of maximum depth all do not correlate with the properties of the liquids. For both liquids approximately the same curves are obtained, both showing only a clear dependency on the phase of the wave. It can therefore be concluded that for impingements upon large amplified surface waves the influence of the viscosity on the time evolution of the depth of the cavity is only minor and therefore can be neglected. This means that the small differences between the results for both liquids, observed in Figure 5.31(b), can only be the result of the difference in terminal velocity of the impinging drops, because of the equal value of the surface tension for both liquids.

Time evolution of the diameter of the cavity

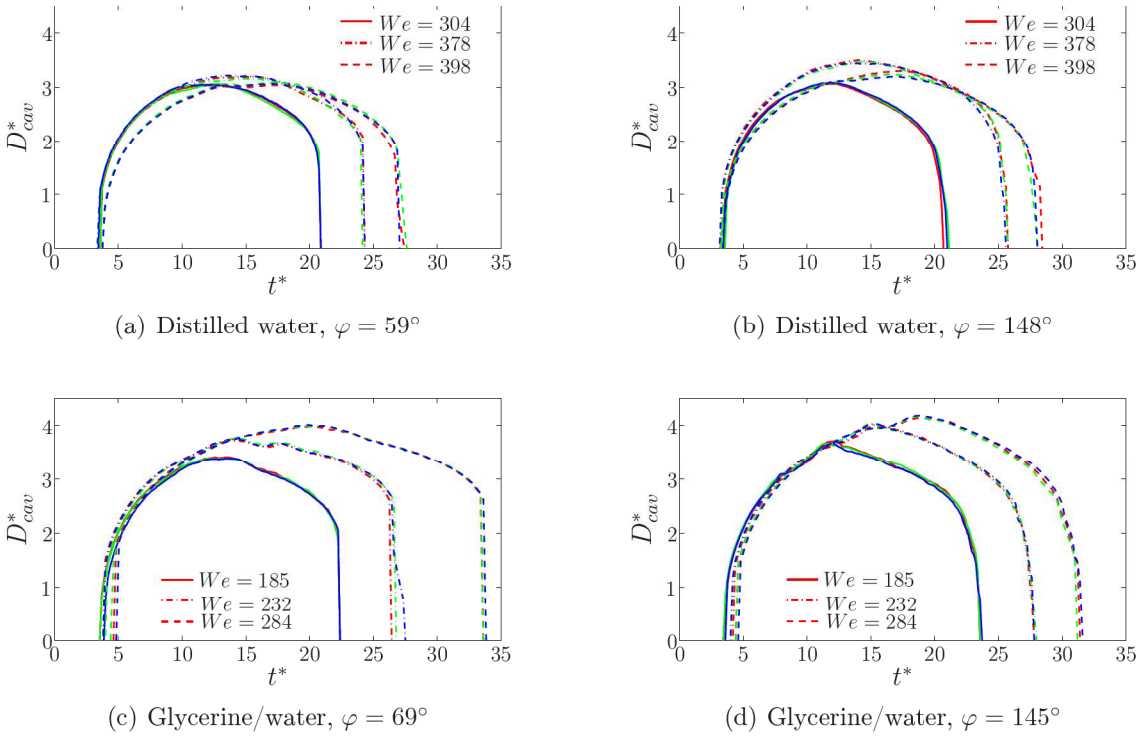

(a) Distilled water, $\varphi = 59°$

(b) Distilled water, $\varphi = 148°$

(c) Glycerine/water, $\varphi = 69°$

(d) Glycerine/water, $\varphi = 145°$

Figure 5.32: Repeatability study for the single drop impingement onto different phases of the small amplified wave for distilled water and glycerine/water. The impingement parameters are listed in Table 3.2 and 5.2

In order to verify the repeatability of the single drop impingement processes on the outcome of the time evolution of the diameter of the cavity, several time evolutions of the diameters of the cavity for different phases of the wave upon impingement are shown in Figure 5.32 and in

Figure 5.33 for respectively the impingement upon the small and large amplified solitary wave. In each of these figures the results for the three investigated absolute Weber numbers, defined by the velocity of the impinging drop and of the surface wave, are presented.

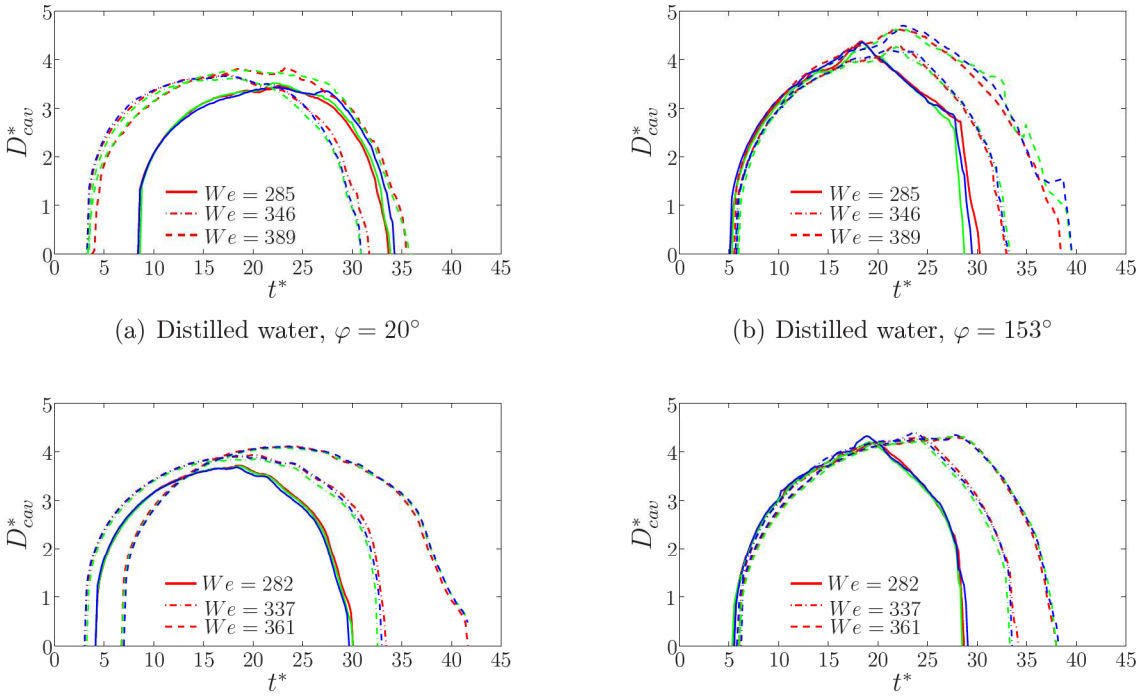

(a) Distilled water, $\varphi = 20°$

(b) Distilled water, $\varphi = 153°$

(c) Glycerine/water, $\varphi = 26°$

(d) Glycerine/water, $\varphi = 150°$

Figure 5.33: Repeatability study for the single drop impingement onto different phases of the large amplified wave for distilled water and glycerine/water. The impingement parameters are listed in Table 3.2 and 5.2

Just as for the presentation of the results for the time evolution of the depth of the cavity, also here a very high repeatability of the impingement process is observed for all measurements. The mean spreading of the diameter evolution in time is presented in Table 5.3, where it is noted that for the diameter evolution the spreading is larger than for the depth evolution, but lies for most of the cases still below 5%. Also for the time evolution of the diameter it is therefore justified that for the discussion presented hereafter the mean diameter evolution is taken over the five repeated measurements.

The first parameter, which influences are studied on the time evolution of the diameter of the cavity, is the phase of the solitary surface wave upon impingement. Plots of the absolute non-dimensional cavity diameter against the non-dimensional time upon different phases of the waves are given in Figure 5.34 for the small amplified wave and in Figure 5.35 for the large amplified wave.

In each figure the results for two of the three investigated absolute Weber numbers, based on the combined velocity of the impinging drop and the solitary surface wave, are presented for both investigated liquids. In the same figure, the relative diameter of both sides of the cavity is presented as well. This relative diameter is measured from the vertical axis going through the center of the drop at impingement to the left and right side of the cavity. The values of

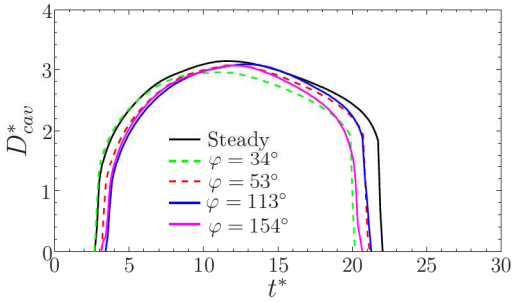

(a) Distilled water, absolute diameter ($We = 304$, $Re = 10,411$)

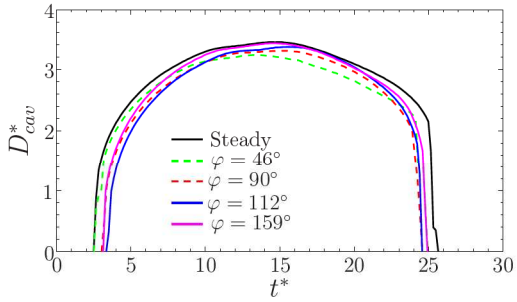

(b) Distilled water, absolute diameter ($We = 378$, $Re = 11,611$)

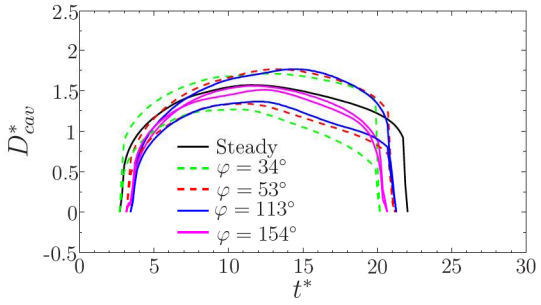

(c) Distilled water, relative diameter ($We = 304$, $Re = 10,411$)

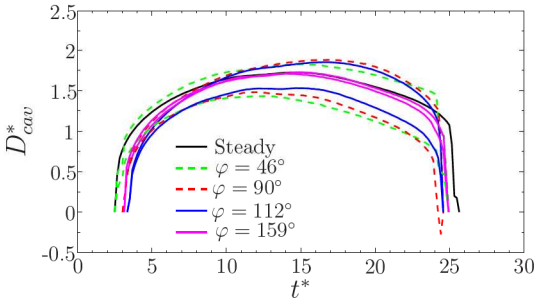

(d) Distilled water, relative diameter ($We = 378$, $Re = 11,611$)

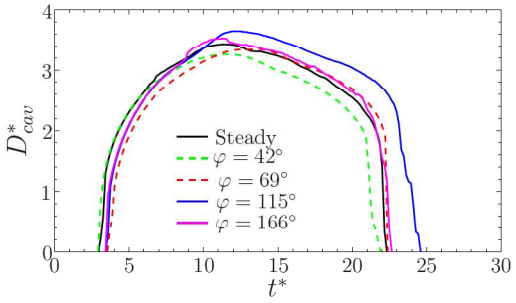

(e) Glycerine/water, absolute diameter ($We = 185$, $Re = 7,276$)

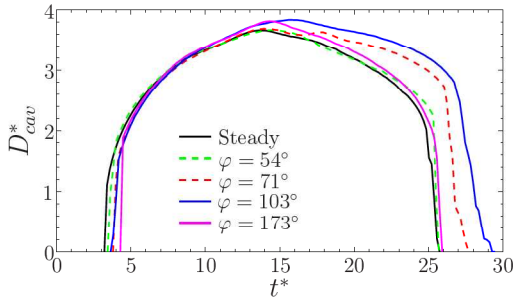

(f) Glycerine/water, absolute diameter ($We = 232$, $Re = 8,191$)

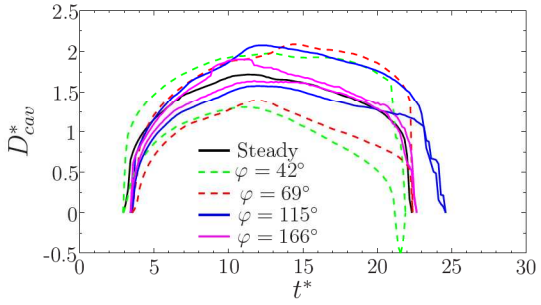

(g) Glycerine/water, relative diameter ($We = 185$, $Re = 7,276$)

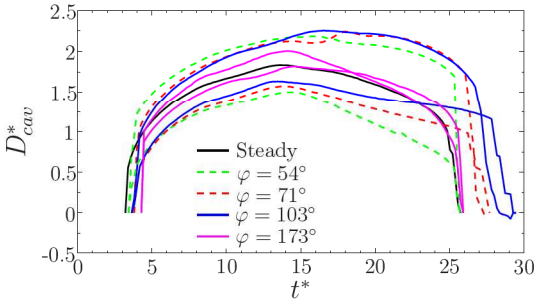

(h) Glycerine/water, relative diameter ($We = 232$, $Re = 8,191$)

Figure 5.34: Evolution of the absolute and relative diameter of the cavity in time as a function of the phase of the wave upon impingement onto the small amplified wave. Comparison of the experimental results for different Weber numbers and liquids. The impingement parameters are listed in Table 3.2 and 5.2

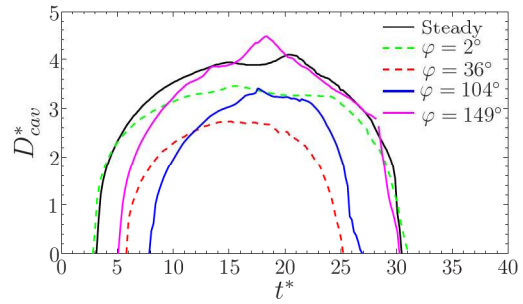

(a) Distilled water, absolute diameter ($We = 285$, $Re = 9,170$)

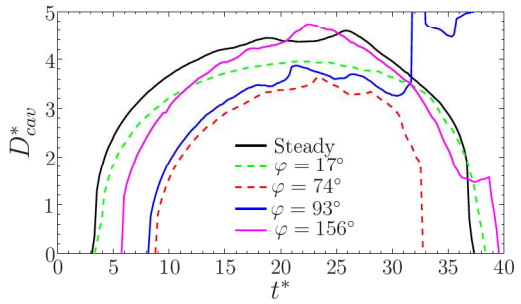

(b) Distilled water, absolute diameter ($We = 389$, $Re = 10,796$)

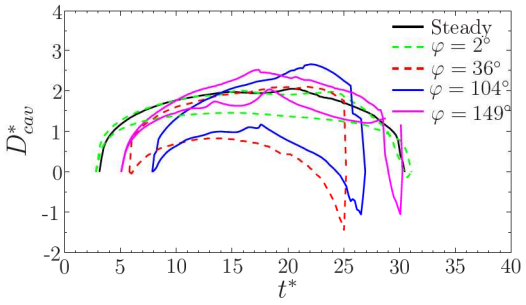

(c) Distilled water, relative diameter ($We = 285$, $Re = 9,170$)

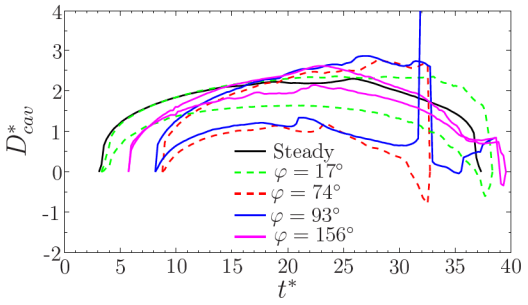

(d) Distilled water, relative diameter ($We = 389$, $Re = 10,796$)

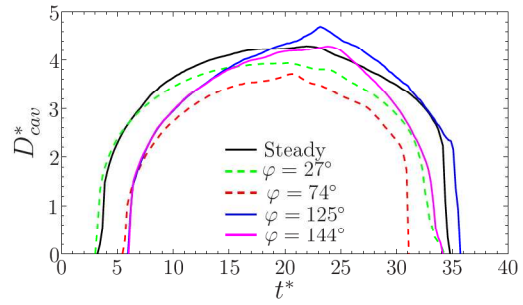

(e) Glycerine/water, absolute diameter ($We = 337$, $Re = 9,873$)

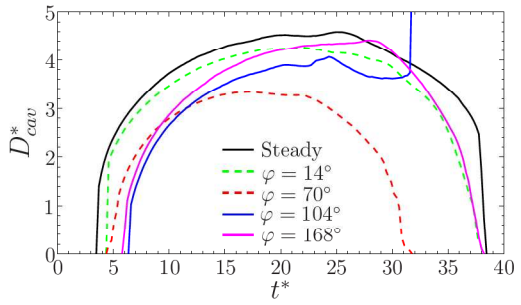

(f) Glycerine/water, absolute diameter ($We = 361$, $Re = 10,112$)

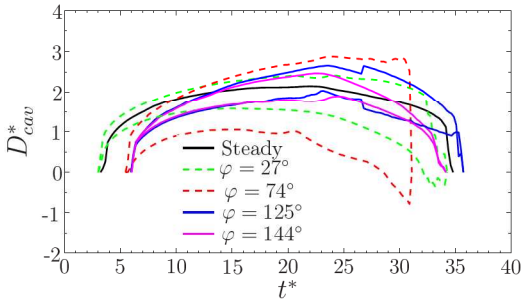

(g) Glycerine/water, relative diameter ($We = 337$, $Re = 9,873$)

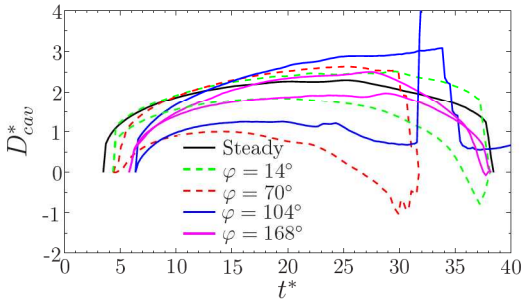

(h) Glycerine/water, relative diameter ($We = 361$, $Re = 10,112$)

Figure 5.35: Evolution of the absolute and relative diameter of the cavity in time as a function of the phase of the wave upon impingement onto the large amplified wave. Comparison of the experimental results for different Weber numbers and liquids. The impingement parameters are listed in Table 3.2 and 5.2

the relative diameters at both sides of the cavity give an indication of the symmetry of the cavity relative to the point of impingement. In case of an absolute symmetrical cavity during the expansion, receding and contraction phases, the relative diameters at both sides are equal, leading to one single curve. However, when the cavity expands faster at one side, the curve belonging to this particular side will lie above the curve belonging to the other half side of the cavity. As a reference for each case, the time evolution of the diameter for the impingement upon a steady liquid surface film of equal thickness is shown as well, which shows a perfectly symmetrical diameter of the cavity during all phases.

Looking at the curves for the absolute diameter of the cavity in time upon the impingement onto the small amplified wave, Figure 5.34, it is seen that for distilled water only a minor change of the diameter evolution in time occurs for the different wave-phases and that all curves follow approximately the reference curve for the impingement onto a steady liquid film. Although it was seen in Figure 5.22 that the phase of the wave and thus the inclination of the film surface, has a distinct influence on the depth evolution of the cavity in time, only a minor influence of the inclination of the surface on the absolute diameter is observed.

For the glycerine/water mixture, however, a stronger change of the diameter evolution is seen between the different phases of the wave. During the expansion phase of the cavity, which takes place between $3 \leq t^* \leq 11$ and between $3 \leq t^* \leq 15$ for respectively $We = 185$ and $We = 232$, no influence of the inclination of the surface is observed. At the time instant at which all kinetic energy, available upon impingement, is converted into surface tension energy and dissipated energy, the maximum diameter of the cavity is reached. The values of the maximum diameter for all investigated phases, Weber numbers and liquids are shown in Figure 5.36(a). It is observed that for all investigated Weber numbers the maximum diameter is independent of the wave-phase. The value of the constant maximum diameter, however, increases weakly for larger Weber numbers and correlates with the liquid properties. For distilled water the values of the maximum diameter lie inbetween $3.0 \leq D^*_{cav,max.} \leq 3.4$ and for glycerine/water inbetween $3.4 \leq D^*_{cav,max.} \leq 4.0$. This difference results from the higher value of the viscosity for glycerine/water, due to which the expansion of the cavity is influenced more by the surface wave itself, as will be explained in detail later in this section.

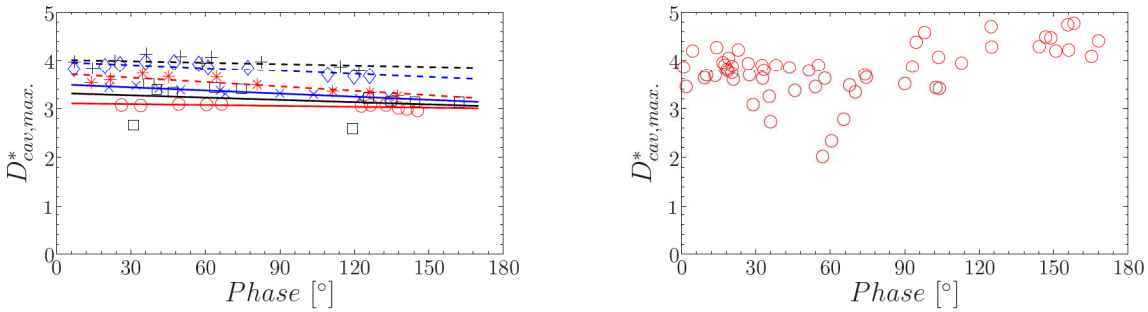

(a) Small wave (b) Large wave

Figure 5.36: Maximum diameter of cavity, measured at half its maximum depth, as a function of the phase of the wave upon impingement for both wave amplifications. The symbols in image (a) represent: Distilled water: We = 303 (◯), We = 378 (×) and We = 398 (□); Glycerine/water: We = 184 (★), We = 232 (◊)and We = 284 (+))

The time instant at which this maximum diameter of the cavity is reached is plotted in Figure 5.37 against the phase of the wave upon impingement. For both liquids an approximately

constant value of the time instants, at which the maximum diameter of the cavity occurs, is observed for all phases of the wave. It is seen that for an increase of the Weber number a later time instant is reached, which is expected because of the higher amount of kinetic energy present upon impingement, as will be explained in detail later on in this chapter.

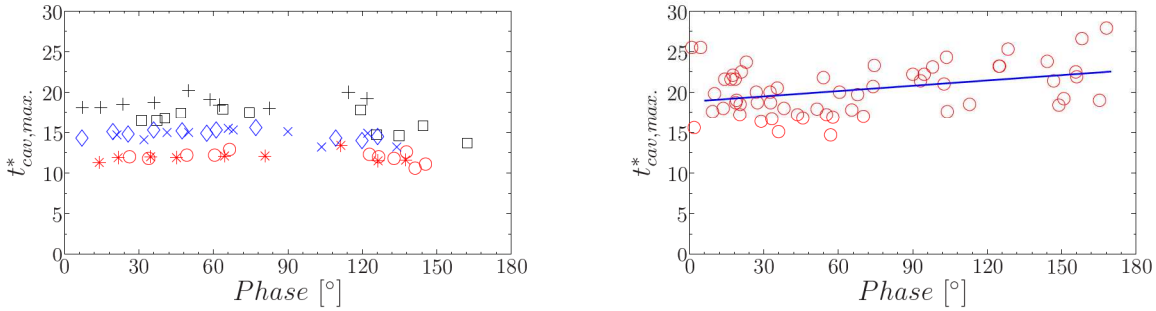

(a) Small wave (b) Large wave

Figure 5.37: Time to reach maximum diameter of cavity, measured at half its maximum depth, as a function of the phase of the wave upon impingement for both wave amplifications. The symbols in image (a) represent: Distilled water: We = 303 (◯), We = 378 (×) and We = 398 (□); Glycerine/water: We = 184 (★), We = 232 (◊)and We = 284 (+))

During the receding phase of the cavity a more distinct dependency of the phase of the wave is observed for the glycerine/water mixture, Figure 5.34(e) and 5.34(f). This can be explained by looking at the time evolution of the relative diameter at both sides of the cavity, Figure 5.34(g) and 5.34(h). Due to the impingement of the drop onto an inclined surface the expanding rim interacts with either the leading edge or the trailing edge of the surface wave, depending on the time instant of impingement. As a result of this interaction, the rim is formed in an asymmetrical way, its asymmetry correlating directly with the steepness of the surface. Together with the motion of the wave from the right to the left, this leads to a cavity that expands radially in an asymmetrical way as well. At the time instant at which this radially expanding cavity passes the vertical position where the diameter of the cavity is measured, the shape of the cavity is therefore already different at both sides for most of the investigated phases of the wave, as can be seen clearly in Figure 5.34(g) and 5.34(h). The rate with which the diameters at both sides of the cavity increase, depends on the phase of the wave and the direction in which the waves travel through the liquid pool. Because of the left-directed motion of the solitary wave, the cavity propagates into this direction during its expansion phase, resulting in a relatively larger expansion of the left side of the cavity seen from the point of impingement. The right side of the cavity expands in the opposite direction as the propagation of the solitary surface wave, resulting in a faster conversion of the kinetic energy at this side and thus a smaller relative diameter appears. Therefore, in all figures presented in this chapter the curve for the left relative diameter lies above the curve for the right side during the expansion phase of the cavity. The velocity of the small surface wave, however, is relatively small in comparison to the impinging velocity of the drop, due to which the amount of asymmetry, caused by the horizontal motion of the cavity, is minor.

For the impingement on the wave-phases between approximately $40 \leq \varphi \leq 75$ a strong interaction of the right side of the rim with the leading edge of the surface wave occurs, due to which a lower rim is formed at this side. At this side of the cavity the gravity forces overcome earlier the kinetic energy, leading to an earlier merging of the right side of the rim with the

surface film, hence an earlier formation of the capillary wave at this side of the cavity. The downward motion of this capillary wave, together with the motion of the liquid and the increasing surface tension forces that oppose the expanding of the cavity, leads to an earlier time instant at which the maximum diameter at the right side of the cavity is reached in comparison to the left side of the cavity, which can expand freely. This can be seen clearly by looking at the curves for $\varphi = 42°$ and $\varphi = 69°$ (Figure 5.34(g)) and for $\varphi = 54°$ and $\varphi = 71°$ (Figure 5.34(h)). For wave-phases between approximately $100 \leq \varphi \leq 140$ this interaction occurs at the left side of the rim, but has the same effect, leading to an earlier appearance of the left capillary wave, see $\varphi = 115°$ (Figure 5.34(g)) and $\varphi = 103°$ (Figure 5.34(h)). For these two wave-phases, however, the difference between the relative diameter at both sides of the cavity is smaller in comparison to the results for $\varphi \leq 90°$, due to the weaker inclination of the trailing edge of the cavity, thus a weaker interaction of the rim with the surface of the wave. For the highest wave-phases shown for glycerine/water, the differences between both sides of the cavity are only minor and lie close to the curve for the reference measurement.

With the use of the differences in the relative diameter at both sides of the cavity, the more distinct dependency of the phase of the wave on the receding of the cavity for the glycerine/water mixture, Figure 5.34(e) and 5.34(f), can be explained. Because of the early formation of the capillary wave at the right side of the cavity, leading to large differences between the relative diameters for $\varphi = 42°$ (We = 185) and $\varphi = 54°$ (We = 232), the receding motion of the cavity is faster, hence a steeper curve of the diameter evolution of the cavity is observed in Figure 5.34(e) and 5.34(f) for these two phases. For increasing wave-phases the interaction of the rim with the leading or trailing edge of the surface wave becomes weaker, resulting in a later formation of the capillary waves, hence the differences between the curves for the relative diameters gets smaller, and therefore a less steep decrease of the absolute diameter during the receding phase of the cavity, compare for example the curve for $\varphi = 103°$ with $\varphi = 54°$ in Figure 5.34(f). For very high wave-phases, close to $\varphi = 180°$ the interaction with the surface wave is negligible, leading to a diameter evolution in time that equals the diameter evolution for the reference case.

For distilled water the same observations can be made. For low phase angles a very distinct difference in the relative diameters for both sides are observed, which become smaller for increasing phase angles. The lower values of the viscosity for distilled water lead, for the same phase angle, to a lower difference between both relative diameters compared to glycerine/water, meaning that the cavities for distilled water are more symmetrical, hence the capillary waves are formed at both sides of the cavity around the same time instant. This explains the minor differences seen between the curves of the absolute diameter for different wave-phases during the receding phase of the cavity.

The results of the time evolution of the diameter of the cavity for the impingement upon large amplified waves show distinct differences, depending on the liquid properties and thus indirectly on the amplification of the wave. The discussion will therefore be split up into two parts, where hereafter first the results of the impingements for distilled water will be analysed, followed by those for the glycerine/water mixture.

Figure 5.35(a) and 5.35(b) show distinct differences between the changes of the diameter in time for different wave-phases; the trends of the curves for the investigated Weber numbers, however, are equal for approximately the same wave-phases. For the discussion of the results, it has to be noted again, that the solitary surface wave propagates from the right to the left. This means that the right side of the cavity expands in the opposing direction of the motion of the liquid. In combination with the increasing surface tension forces, opposing the further

expansion of the cavity, the energy conversion at this side takes place faster than at the left side of the cavity. Its relative diameter will therefore always be smaller than the relative diameter at the left side of the cavity.

For distilled water it is observed in Figure 5.35(a) that for very low wave-phases, like $\varphi = 2°$, the influence of the capillary wave is not felt at the first time instants after impingement, hence the curve for the absolute and relative diameters follow the reference curve. During the expansion of the cavity, the right side of the cavity expands in the opposite direction of the motion of the liquid, which, in combination with the increasing surface tension forces, leads to a very soon energy conversion, seen by the leveling of the curve for the right relative diameter, Figure 5.35(c). At the left side of the cavity, a strong capillary wave is formed soon after impingement, due to which the curve for the left relative diameter also levels off. This leads to an earlier leveling of the curve for the absolute diameter and therefore an increasing difference between the absolute diameters for $\varphi = 2°$ and the reference case. This left capillary wave initiates a distinct merging of the cavity for $t^* > 24$, whereas the capillary wave at the right side of the cavity is not formed before $t^* \approx 27$. Due to the time-delayed formation of the capillary waves at both sides of the cavity, the left side of the cavity recedes much earlier and faster, leading to a crossing of the curves for the relative diameters at $t^* \approx 28$.

For increasing wave-phases, $\varphi = 17°$ (Figure 5.35(b)) and $\varphi = 36°$ (Figure 5.35(a)) a strong asymmetrical formation of the corona is observed upon impingement. The right side of the expanding rim interacts with the oncoming leading edge of the surface wave, whereas the left side of the rim expands freely, thereby forming a pronounced corona. During the expansion phase of the cavity, its inclination to the left increases steadily with time, as a result of the motion of the top of the cavity with the solitary surface wave. In combination with the expansion of the right side of the cavity against the motion of the liquid and the increasing surface tension forces, acting on the cavity, the expanding rate of the relative diameter at this side decreases, Figure 5.35(d) and 5.35(c). Due to the inclination of the cavity, the rim at the left side of the cavity interacts with the surface wave at approximately $t^* = 13$, leading to the direct formation of a strong capillary wave, at which moment the receding of the cavity is initiated at the left side of the cavity. During the receding phase, the left side of the cavity decreases in diameter, whereas the shape of the cavity at the right side remains unchanged. It can be seen in the Figures 5.35(c) and 5.35(d) that for $t^* = 21$ and $t^* = 36$ the values of the relative diameter of the left side of the cavity become negative for respectively $\varphi = 36°$ and $\varphi = 17°$. This means that the left side of the cavity has crossed the symmetry line, hence the receding of the cavity occurs in a distinct asymmetrical way.

For wave-phases around $\varphi = 90°$ the drop impinges onto the top of the solitary surface wave. This leads to a free expansion of the rim and the pronounced formation of the corona. The cavity expands in both directions, but in a strong asymmetrical way. The motion of the liquid, in combination with the increasing surface tension forces, opposes the bright expansion of the cavity at the right side. At the left side, however, the cavity expands far more, due to the distinct motion of this side of the cavity with the liquid. This results in a very large difference between the values of the relative diameters at both sides of the cavity, as can be seen for $\varphi = 104°$ in Figure 5.35(c) and for $\varphi = 74°$ and $\varphi = 93°$ in Figure 5.35(d). This difference increases with time, resulting in a very wide cavity, having a relatively small depth, as can be seen in Figure 5.23(a) and 5.23(b). For these wave-phases the capillary wave at the left is formed a few non-dimensional time instants before the right capillary wave, leading to an asymmetrical receding. For $\varphi = 93°$ the right side of the cavity merges with the trailing edge of the surface wave, due to which no further analysis of the data for this measurement

are possible. For $\varphi = 74°$ and $\varphi = 104°$ is is observed that the capillary wave at the right side of the cavity is formed at the moment the cavity is retracting already, leading to a very pronounced asymmetrical receding and retraction of the cavity.

The impingement occurs for relatively high wave-phases at the trailing edge of the surface wave, resulting in a strong interaction of the left side of the expanding rim with the trailing edge of the wave. The right side of the rim can expand freely, leading to the formation of the corona at this side. The expansion of the cavity is approximately symmetrical, as can be observed in the Figures 5.35(a) to 5.35(d) for $\varphi = 149°$ and $\varphi = 156°$. For these wave angles the curves of the absolute and relative diameters lie very close to the reference curves. Due to the smaller rim at the left side of the cavity, the capillary wave is formed earlier at this side of the cavity, which is observed clearly in the Figures 5.9 to 5.11 for $\varphi = 149°$. Because of the increased height of the surface film at the left side of the cavity, the left capillary wave has to travel a longer distance to the bottom of the cavity. At the moment the left capillary wave reaches the height of the surface film at the right side of the cavity, the rim at this side merges with the surface film, leading to the formation of the right capillary wave. From this time instant on the receding of the cavity is equal at both sides of the cavity, which can be seen clearly by looking at the values of the relative diameters for both sides of the cavity.

The results for the glycerine/water mixture also show a very distinct behaviour depending on the phase of the wave at impingement. For very low phases, hence $\varphi = 14°$ in Figure 5.35(f) and $\varphi = 27°$ in Figure 5.35(e), a corona is formed at both sides of the cavity, however being more pronounced at the left side. Right upon impingement an expanding cavity is formed, which is inclined to the left. A combination of the increase of the inclination of the cavity in time and the expanding motion of the cavity leads to larger values of the relative diameter of the right side of the cavity than would be observed without this inclination of the cavity. This leads to smaller differences between the relative diameters at both sides of the cavity, as is observed in Figure 5.35(g) and 5.35(h) for, respectively, $\varphi = 27°$ and $\varphi = 14°$. As a result of the increased inclination of the cavity in time, the left side of the rim merges earlier with the surface wave, thereby forming the left capillary wave. Because of the absence of the capillary wave at the right side of the cavity, a distinct asymmetrical merging of the cavity occurs, which is observed in Figure 5.35(g) and 5.35(h) as an increase in the differences of the relative diameters between both sides of the cavity. For both wave-phases the curve for the relative diameter at the left side reaches negative diameters at the final stages of the merging of the cavity and the beginning of the cavity retraction.

An increase of the wave-phases leads to the free formation of the rim and corona at both sides of the cavity upon impingement. Due to the distinct motion of the solitary surface wave and the liquid, the left side of the expanding cavity penetrates relatively fast into the liquid film. The right side of the cavity, however, has to oppose during the expansion phase the increasing surface tension forces and the motion of the liquid film, leading to a relatively fast leveling of the curve for the relative diameter at this side, see the curves for $\varphi = 74°$ in Figure 5.35(g) and $\varphi = 70°$ and $\varphi = 104°$ in Figure 5.35(h). A combination of both phenomena leads to an elongated cavity and therefore to a distinct difference between the relative diameters at both side of the cavity. As a result of the motion of the left side of the rim, no merging of the rim with the liquid surface film is seen to occur, hence only a capillary wave at the right side of the cavity is formed. The receding of the cavity is therefore highly asymmetrical; the right side of the cavity changes its shape drastically, whereas the shape at the left side remains unchanged. This leads to an earlier retraction of the cavity, Figure 5.23(c) and 5.23(d).

The impingement on the trailing edge of the solitary surface wave leads to the free formation

of the corona, which interacts at the left side with the trailing edge of the receding solitary wave. The amount of interaction depends on the phase of the wave and thus on the inclination of the trailing edge surface. For steeper inclinations the interaction of the left side of the corona with the surface wave is stronger. The expansion of the cavity occurs symmetrically in a relative high amount, as is observed in the Figures 5.23(c) and 5.23(d) for, respectively, $\varphi = 125°$ and $\varphi = 144°$ and $\varphi = 168°$ and at the Shadowgraph images of the impingement process, presented in the Figures 5.12 to 5.14 for $\varphi = 144°$. Due to the interaction of the rim with the surface film, the capillary wave is formed earlier at this side of the cavity, although the time differences in formation between both capillary waves are not more than a few non-dimensional time instants. This leads therefore to a receding of the cavity, which is approximately symmetrical and equal for all the wave-phases.

Concerning the typical time and length scales associated with the single drop impingement onto liquid films, the values of the maximum absolute diameter and the time instants at which these maximum absolute diameters are reached, are presented as a function of time in, respectively, Figure 5.36(b) and 5.37(b). No clear dependency of the maximum absolute diameter on the phase of the wave upon impingement is found, although for phases around $\varphi \approx 60°$ a slight decrease of the maximum diameters is observed. This is in agreement with the results of the time evolution of the absolute and relative diameters presented in Figure 5.35. In this figure, a slightly lower maximum absolute diameter is observed for each investigated Weber number and liquid, as well as a maximum difference between the relative diameters for both sides of the cavity. The times at which the maximum absolute diameters are reached correlate linearly with the phases of the wave at impingement. For increasing wave-phases the maximum absolute diameter is reached at a later time instant, which can be explained by a weaker interaction of the expanding rim with the surface of the wave for higher wave-phases, leading to a later formation of the capillary waves and thus a later receding of the cavity.

The change of the time evolution of the absolute and relative diameters is presented in Figure 5.38 and C.1 as a function of the absolute Weber number upon impingement onto the small amplified solitary surface wave. Figure 5.38 shows the evolution of the absolute diameter for all three investigated Weber numbers for distilled water and glycerine/water, whereas in Figure C.1 the time evolution of the relative diameters at both sides of the cavity are shown.

When comparing the time evolutions of the absolute diameter of the cavities for the different Weber numbers, it is observed that both for distilled water and for the glycerine/water mixture the same trends are seen. The cavity, which is formed upon impingement, expands for all Weber numbers, wave-phases and for both liquids with the same absolute rate. For increasing Weber numbers more kinetic energy is available upon impingement, due to which this kinetic energy can overcome the increasing surface tension forces, acting on the cavity during its expansion, for a longer time. The cavity can therefore expand longer in radial direction, due to which a wider cavity is formed. The values of the maximum diameter of the cavity and the times at which these maximum diameters are reached, are shown respectively in Figure 5.39(a) and 5.40(a) as a function of the absolute Weber number of the impinging drop.

These figures clearly show a linear increase of the maximum diameter and the time instant of maximum diameter for larger values of the impinging Weber number. It is noted that for the same Weber number the values of both parameters are higher for the glycerine/water mixture than for distilled water. This is explained by investigating the time evolutions of the relative diameters at both sides of the cavity, Figure C.1. The column at the left side of this figure shows the results for three phases of the surface wave for distilled water, whereas at the right side the results are plotted for glycerine/water. For all three wave-phases the same differences

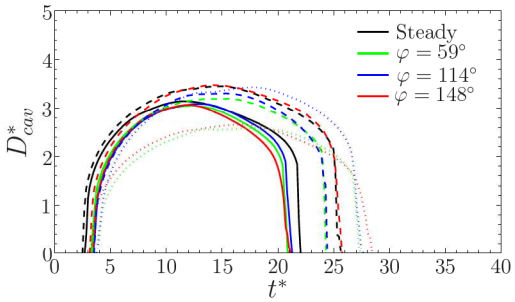

(a) Distilled water, small wave

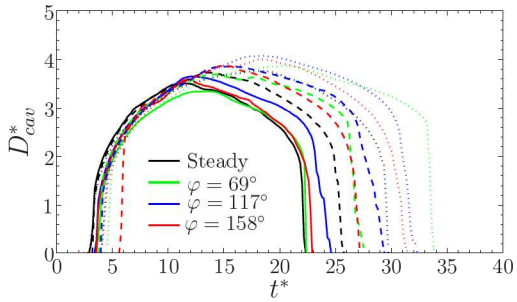

(b) Glycerine/water, small wave

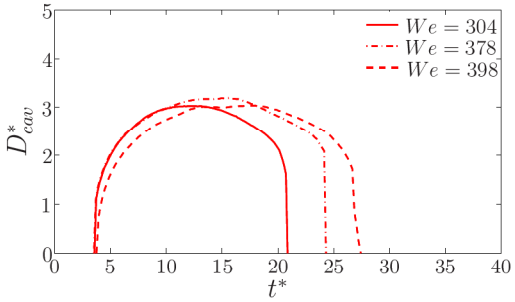

(c) Distilled water, $\varphi = 59°$

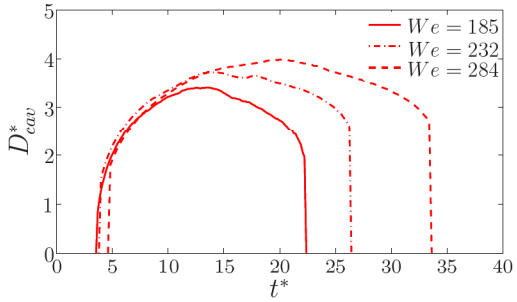

(d) Glycerine/water, $\varphi = 69°$

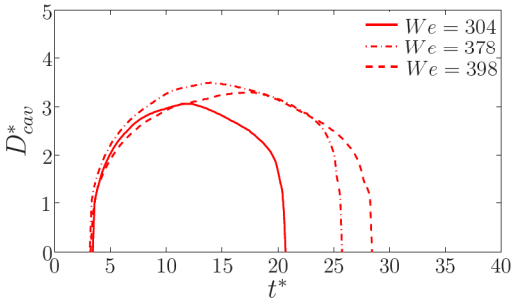

(e) Distilled water, $\varphi = 148°$

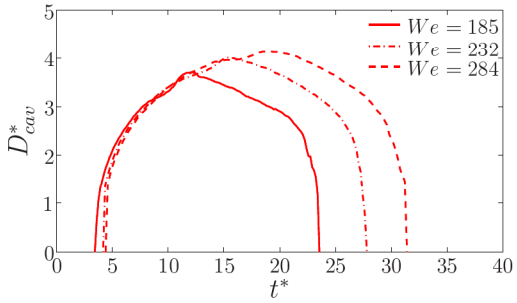

(f) Glycerine/water, $\varphi = 145°$

Figure 5.38: Evolution of the absolute diameter of the cavity in time as a function of the different Weber numbers for the impingement onto the small amplified wave. Comparison of the experimental results for different liquids and wave phases. For figure (a) and (b) the lines represent: lowest Weber number (solid lines), medium weber number (dashed lines) and highest Weber number (dotted lines)

between the curves for both liquids are observed. When focussing on the results for the lowest wave-phase shown, it is observed that for all three investigated Weber numbers the curves for the relative diameter at the right side of the cavity level off earlier for both liquids. Due to the motion of the expanding cavity at this side, which is opposite to the motion of the surface wave, and the increasing surface tension forces, acting on the cavity, the kinetic energy at the right side of the cavity is taken over by the surface tension forces at an earlier time instant.

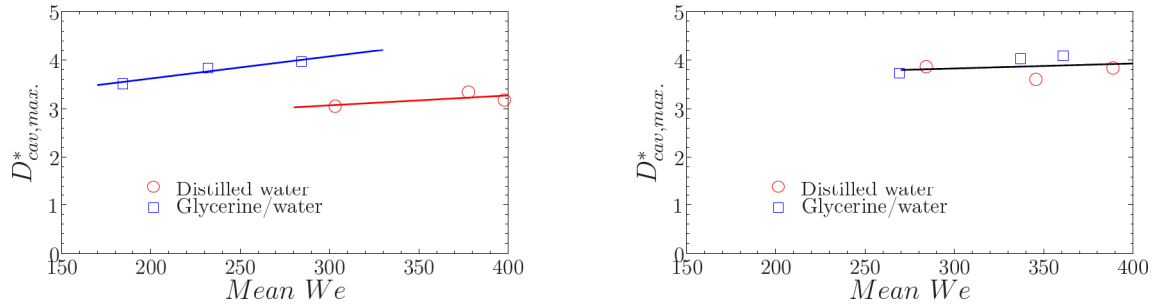

(a) Small wave (b) Large wave

Figure 5.39: Maximum diameter of the cavity, measured at half its maximum depth, as a function of the mean Weber number of the impinging drop for both wave amplifications

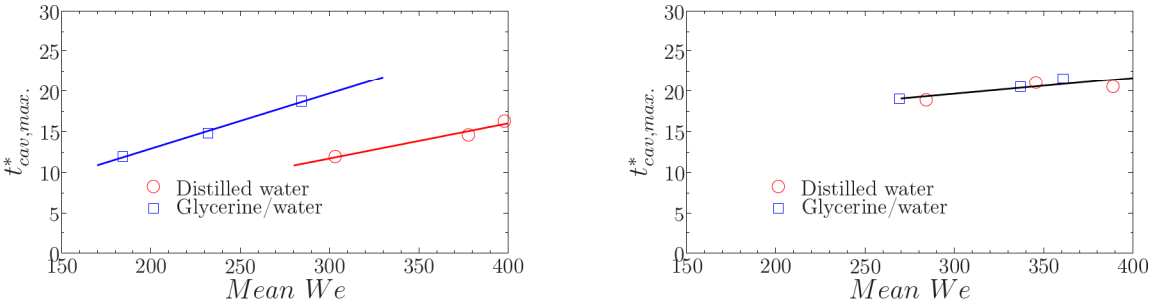

(a) Small wave (b) Large wave

Figure 5.40: Time to reach the maximum diameter of the cavity, measured at half its maximum depth, as a function of the mean Weber number of the impinging drop for both wave amplifications

For the left side of the cavity, however, a strong difference in the curves is seen between both liquids. Because of the higher viscosity of the glycerine/water mixture, the expansion of the cavity at the left side is enhanced by the motion of the surface wave, which is in the same direction. This leads to a later time instant at which the surface tension forces can overcome the expanding motion of the cavity, due to which at this side the values of the relative diameters are larger for glycerine/water. This leads to a larger value of the absolute diameter of the cavity and a later time instant at which this value is reached. The same trend is seen to occur for the other wave-phases, although for larger wave-phases the differences between both liquids become smaller, due to the weaker interactions of the expanding rim and cavity with the surface wave. These weaker interactions lead to the lower time lag between the formation of the capillary waves at both sides of the cavity, due to which a more symmetrical expansion and receding of

the cavity occurs, as has been explained in detail in the paragraph above. In Figure C.1 this is observed as a smaller difference between the curves of the relative diameters at both sides of the cavity for higher values of the phase of the wave, compare for example the curves in Figure C.1(a) and C.1(b) with respectively the curves in Figure C.1(e) and C.1(f).

For the impingement onto the large amplified surface wave the changes of the time evolutions of the absolute and relative diameters are presented in Figure 5.41 and C.2 as a function of the absolute Weber number. The first figure shows the evolution of the absolute diameter for all three investigated Weber numbers for distilled water and glycverine/water, whereas in the latter figure the time evolution of the relative diameters at both sides of the cavity are plotted.

The time evolutions of the absolute diameters for both liquids show, just like for the impingement onto steady liquid surface films and small amplified surface waves, a clear correlation with the Weber number, but the differences are less pronounced. The expansion rate of the cavities upon impingement changes only in a minor way between the different investigated Weber number and is furthermore independent of the phase of the wave, Figure 5.41. Due to the higher value of the kinetic energy for increasing Weber numbers, the increasing surface tension forces, acting on the cavity during its expansion, can be overcome for a longer time. The radial expansion of the cavity lasts therefore over a longer time period, resulting in a wider cavity, although the differences between the curves for the absolute diameter of the cavities are smaller than was observed for the impingement onto the small amplified wave. The values of the maximum diameter of the cavity and the time at which this maximum diameters is reached, are shown respectively in Figure 5.39(b) and 5.40(b) as a function of the absolute Weber number of the impinging drop.

In Figure 5.39(b) it is seen that the maximum values of the absolute diameter are approximately constant for the mean absolute Weber numbers and that the differences between the two liquids, present for the small amplified wave (Figure 5.39(a)), have disappeared. This means that for the impingement onto large amplified surface waves, hence solitary waves with a high velocity and maximum amplitude, the influence of the viscosity of the liquid and thus of the Reynolds number on the value of the maximum absolute diameter can be neglected. The same conclusion can be drawn for the time instant at which this maximum diameter is reached, Figure 5.40(b). For this typical time scale a clear linear dependency on the mean Weber number is observed, but no relation with the Reynolds number is seen to occur.

An explanation for this behaviour of the typical time and length scales can be found by analysing the time evolution of the relative diameters of both sides of the cavity, presented in Figure C.2. With the exception of the curves for $\varphi = 102°$ for glycerine water, Figure C.2(f), it is seen that for all shown phases of the wave the curves for the three Weber numbers do not differ much in shape. As expected, the values of the relative diameter of the right side of the cavity are smaller for all wave-phases and Weber numbers than of the left side of the cavity, because of the opposite motion of the right side of the expanding cavity to the motion of the solitary wave and the increasing surface tension forces, opposing the further expansion of the cavity at this side. This results in an earlier time instant at which the surface tension forces overcome the kinetic energy at the right side of the cavity, hence an earlier leveling of the curves of the relative diameter.

For relatively low wave-phases, hence $\varphi = 20°$ for distilled water and $\varphi = 26°$ and $\varphi = 33°$ for glycerine/water, a strong interaction of the right side of the expanding rim with the oncoming leading edge of the surface wave occurs, whereas at the left side a corona is formed upon impingement. During the expanding phase the cavity gets wider, but at the same time its inclination increases to the left, due to the motion of the surface wave in this direction. The expansion of the cavity at the left side is therefore canceled out by the increasing inclination

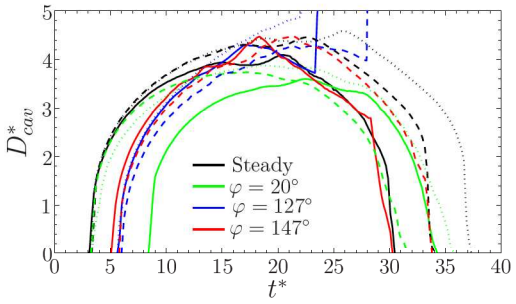

(a) Distilled water, large wave

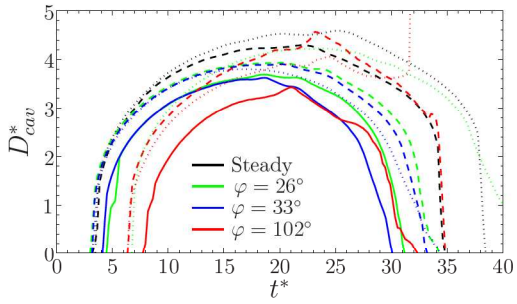

(b) Glycerine/water, large wave

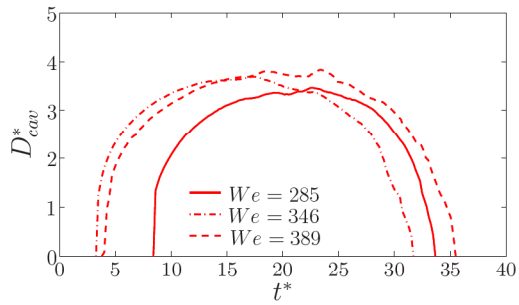

(c) Distilled water, $\varphi = 20°$

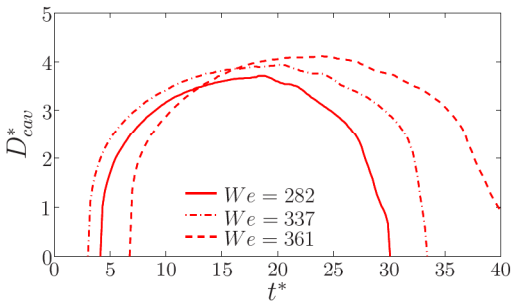

(d) Glycerine/water, $\varphi = 26°$

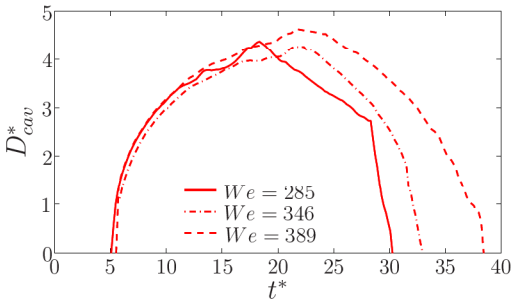

(e) Distilled water, $\varphi = 153°$

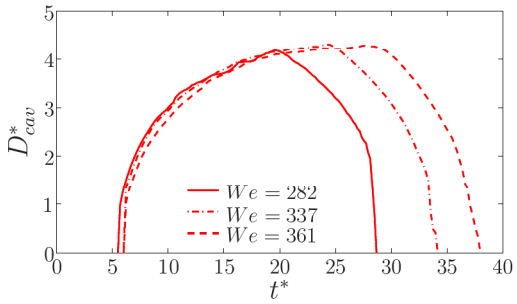

(f) Glycerine/water, $\varphi = 150°$

Figure 5.41: Evolution of the absolute diameter of the cavity in time as a function of the different Weber numbers for the impingement onto the large amplified wave. Comparison of the experimental results for different liquids and wave phases. For figure (a) and (b) the lines represent: lowest Weber number (solid lines), medium weber number (dashed lines) and highest Weber number (dotted lines)

of the cavity, which pushes the left side of the cavity into the right direction. This behaviour can be seen clearly for $\varphi = 20°$ in the Figures 5.3 to 5.5. In Figure C.2(a), C.2(b) and C.2(d) this is observed as an approximately constant value of the relative diameter at the left side of the cavity for all Weber numbers. For increasing Weber numbers, the cavity expands more in radial direction, but simultaneously its inclination increases faster, thereby canceling out the increased expansion. This leads to a relatively small increase of the relative diameter at the left side of the cavity, due to which the maximum absolute diameter changes only in a minor way. The only exception is the curve for $We = 361$ in Figure C.2(b), where the inclination of the cavity is smaller, due to which higher values of the relative diameters at both sides of the cavity are reached. The receding of the cavity occurs for all of these wave angles in the same manner. Due to the inclination of the cavity, the left side of the corona merges earlier with the surface wave, resulting in an earlier formation of the capillary wave at this side. The cavity starts its receding motion at this side, but during the receding phase both the inclination of the cavity and the motion of the cavity with the solitary wave are increased. This leads to a relative diameter at the left side which remains more or less constant, whereas it is observed that the relative diameter at the right side of the cavity decreases fast. The motion of the complete cavity to the left leads therefore to the appearance of negative values of the relative diameter of the right side of the cavity.

For the impingement onto the trailing edge of the wave, hence $\varphi = 127°$, $\varphi = 147°$ and $\varphi = 150°$ for distilled water and $\varphi = 150°$ for glycerine/water, the interaction of the left side of the expanding rim is less pronounced, whereas at the right side of the cavity a corona can be formed. Because the main part of the solitary surface wave has passed the impingement point, the influence of the surface wave on the expanding cavity is less pronounced as well. This leads to a relatively symmetrical expanding of the cavity, resulting in a smaller difference between the values of the relative diameters at both sides of the cavity, Figure C.2(c) and C.2(e). With increasing wave-phase at the trailing edge of the wave, the curves for both relative diameters lie closer to the reference curve. For all the wave-phases it is observed that for the three investigated Weber numbers the capillary wave at the right side is formed at approximately the same time instant, whereas the capillary wave at the left side of the cavity is formed later for larger Weber numbers, compare for example the Shadowgraph images for $\varphi = 149°$ and $We = 293$ (Figure 5.9 to 5.11) with those for $\varphi = 147°$ and $We = 342$ (Figure 5.3 to 5.5). For the lowest investigated Weber number the capillary waves are formed at approximately the same time instant, leading to a symmetrical receding of the cavity, see the solid lines in Figure C.2(c) and C.2(e). Because for increasing Weber numbers the capillary wave at the right side of the cavity is formed earlier than at the left side of the cavity, the receding at the right side is initiated earlier, thereby leveling the curves for the absolute diameter. This leveling takes place over a longer time period for higher Weber numbers, because the left side of the cavity expands over a longer period. This explains the approximately equal values of the maximum absolute diameters for all the Weber numbers and the later time instants at which these maximum values are reached.

Two amplifications of the solitary surface wave are generated, in order to investigate the influence of the velocity and the maximum amplitude of the surface wave on the single drop impingement outcomes. The results of the time evolution of the diameter of the cavity formed upon impingement onto the two investigated wave topologies are shown in Figure 5.42 for glycerine/water. The figure at the left shows the changes of the absolute diameters in time for three phases of the wave, whereas in the right figure the belonging relative diameters of both sides of the cavities are presented.

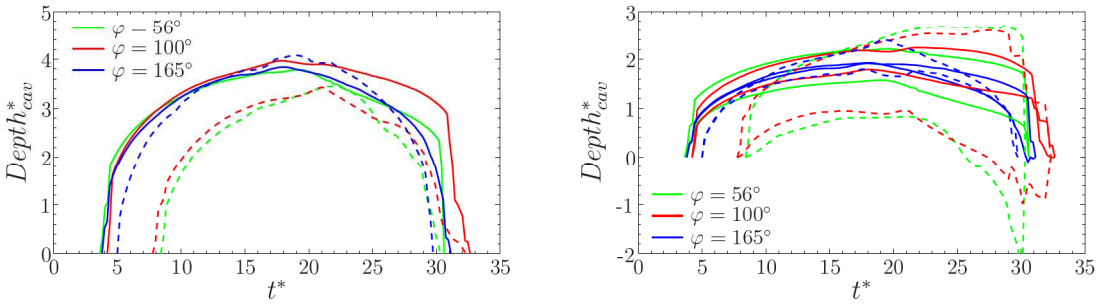

(a) Absolute diameter (b) Relative diameter

Figure 5.42: Evolution of the absolute and relative diameter of the cavity in time for different wave amplifications. Comparison of the experimental results for the single drop impingement onto different phases of the small (solid lines, $We = 284$, $Fr = 316$ and $Re = 8,980$) and large (dashed lines, $We = 285$, $Fr = 296$ and $Re = 9,170$) wave for glycerine/water

During the first part of the expansion phase of the cavity the rate of increase of the absolute diameters are equal for both liquids. For the larger amplified wave, however, it is observed that for $\varphi = 56°$ and $\varphi = 100°$ the increase of the absolute diameter starts to level-off faster than for the small amplified wave. Because of the same Weber number and Reynolds number upon impingement for both surface wave topologies, the difference can only be found by looking at the amplification of the wave itself. For the large amplified wave the surface wave velocity and the maximum amplitude of the wave are about 1.5 times larger. It is therefore expected that the influence of the surface wave on the expansion of the cavity is larger than for the small amplified wave.

In Figure 5.42(b) it can be seen that for these two wave-phases a strong asymmetrical expansion of the cavity occurs right after impingement upon the large surface wave. Due to the motion of the surface wave from left to right and the increasing surface tension forces acting on the expanding cavity, the expansion rate of the cavity at the right side of the cavity is much smaller than at the left side. These phenomena lead to an early time instant at which the kinetic energy at this side of the cavity is overcome by the surface tension forces. For both wave-angles this occurs around $t^* = 21$, at which moment the inclination of the curves changes from positive to negative. At this instant the maximum absolute diameter of the cavity is reached, Figure 5.42(a). The left side of the cavity expands in a stronger way than is the case for the impingement onto a steady liquid surface film, because of the motion of the solitary surface wave, which is in the same direction as the expansion of this side of the cavity. Due to this additional motion of the left side of the cavity, the right side of the rim falls back onto the liquid surface sooner, initiating the formation of the capillary wave at an earlier time instant. The combination of the receding motion of the cavity and the motion of the liquid film leads to a steep decrease of the relative diameter at the right side of the cavity, whereas in the same period the left side of the cavity still increases in diameter. This leads to a very strong asymmetrical receding of the cavity, where the capillary wave at the left side of the cavity is not formed until the cavity has started its retracting motion already.

For the impingement onto the wave-phase $\varphi = 165°$ of the large amplified wave, the influence of the motion of the liquid film is only minor, because the main part of the surface wave has passed the impingement region already at this wave-phase. This leads to relatively minor differences in the expansion of the cavity between both sides and a fairly symmetrical

formation of the capillary waves and subsequent receding of the cavity, Figure 5.42(b). The same observations can be made for the curves of the absolute and relative diameters for the impingements onto the small surface wave, because of the relatively low velocity and amplitude of this wave with respect to the large surface wave. This leads to relatively small influences on the expansion of the cavities at both sides, hence an approximately symmetrical expansion and receding of the cavity occurs.

The last parameters, varied to investigate its influence on the outcomes of the impingement onto the solitary surface waves, are the liquid properties. In this case, only the viscosity of the liquid is changed, the surface tension remains the same. In Figure 5.43 the absolute and relative diameters are shown for the impingement upon the small and large amplified surface wave, where a comparison is made between the shape of the curves for both liquids.

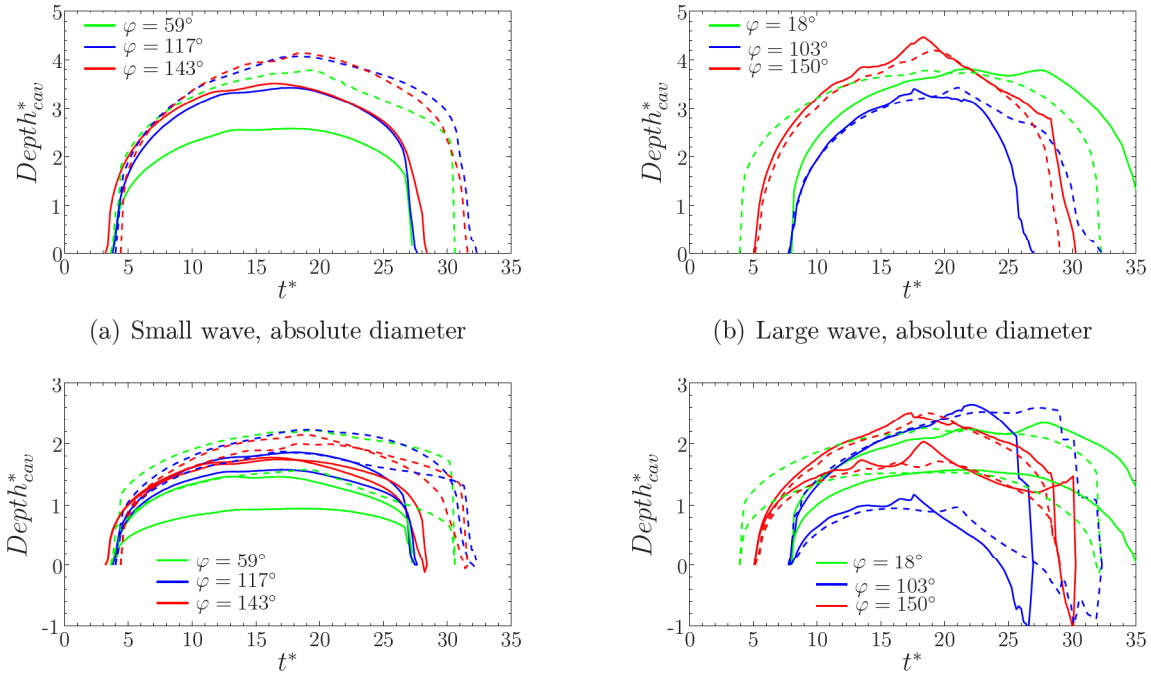

(a) Small wave, absolute diameter

(b) Large wave, absolute diameter

(c) Small wave, relative diameter

(d) Large wave, relative diameter

Figure 5.43: Evolution of the absolute and relative diameter of the cavity in time for different liquids. Comparison of the experimental results for the single drop impingement onto different phases of the small wave (left) and large wave (right) for distilled water (solid lines) and glycerine/water (dashed lines). The impingement parameters are for the small wave $We = 398$ and $Re = 11,458$ (distilled water) and $We = 284$ and $Re = 8,980$ (glycerine/water) and for the large wave $We = 285$ and $Re = 9,170$ (distilled water) and $We = 282$ and $Re = 9,004$ (glycerine/water)

For the small amplified wave it is seen that, with the exception of $\varphi = 59°$ for distilled water, all curves follow the same trend during the expansion phase of the cavity. Due to the larger value of the viscosity for glycerine/water the left side of the cavity is expanded more than for distilled water, as can be seen clearly in Figure 5.43(c). Because of the lower propagation velocity of the solitary wave for glycerine/water, the expansion of the cavity at its right side can continue for longer time instants, before the surface tension forces, acting on the cavity,

overcome the kinetic energy. This results in a wider cavity, hence a larger maximum of the absolute diameter is found for the glycerine/water mixture, as was shown already in Figure 5.36(a). The time instant, at which these maximum values are reached, are, however, approximately the same, Figure 5.37(a), as a result of the approximately same time instant at which the capillary waves are formed. A larger value of the maximum diameter for glycerine/water, in combination with the almost identical value of the surface tension, leads to a longer time period during which the receding of the cavity takes place, and thus a later retraction of the cavity.

Just as for the results of the time evolution of the depth of the cavity for distilled water and glycerine/water, presented in Figure 5.31(b), the same time evolutions of the absolute and relative diameters of the cavity are found for the impingement upon the large amplified wave for both liquids, Figure 5.43(b) and 5.43(d). The differences between the curves for distilled water and glycerine/water for $\varphi = 103°$ are the direct result of the time instant at which the capillary waves are formed at both sides of the cavity. Because the formation of the capillary waves for distilled water is about six non-dimensional time instants earlier at both sides of the cavity, an earlier receding of the cavity occurs for distilled water, leading to an earlier decrease of the absolute diameter for this wave-phase.

The appearance of approximately the same curves for both liquids means that for large amplified waves, hence having a large value of the wave propagation velocity and wave amplitude, the viscosity of the liquid does not play a significant role anymore on the impingement process. This was already concluded by looking at the graphs for the value of the maximum diameter and the time instant at which these maximum diameters are reached, Figure 5.36(b) and 5.37(b), where it was noted that this typical length and time scale are independent of the viscosity. A linear relation was found between the typical time and length scale on one side and the mean Weber number on the other side, leading to the conclusion that the impingement process does depend strongly on the terminal velocity of the impinging drop, because the value of the surface tension is similar for both liquids.

5.3 Summary

The analytical models, applied for the simulation of spray impingement processes, are mostly based on the experimental results of single drop impingements onto steady liquid films. In the best case, the experimental data of the inclined drop impingements are used. Sprays, however, are a collection of a large number of drops, where the outcome of each individual drop impingement onto a liquid film is influenced by the unsteady wall film flow, as well as by the interactions with other impinging drops, both in the spray and during the interaction with the wall film, all of them having a significant effect on the spray impingement process.

In order to show that not only the waviness of the liquid film, but also the velocity and amplitude of the surface film, have a significant influence on the spray impingement outcomes, shadowgraph recordings have been made of the impingements of single drops onto steady liquid surface films of finite thickness and onto solitary surface waves. In the first part of this chapter the observations of these impingements have been presented and compared in detail. The results of the time evolution of the cavity upon impingement onto a solitary surface wave, propagating with a constant velocity through the measurement area, were explored. Here the differences in the cavity evolution for a change in the phase of the wave at the point of impingement between $0° \leq \varphi \leq 180°$, in Weber number of the impinging drop, based on the total impingement velocity vector, in the amplification of the solitary wave (propagation velocity and maximum amplitude) and in the liquid properties (surface tension and viscosity) were described

and explained. Hereafter, only the most important observations will be summarised.

A change in the topology of the liquid surface film has a distinct influence on the outcome of the impingement process and on the time evolution of the cavity shape. The solitary wave induces a relative velocity component onto impingement, due to which the shape and inclination of the corona are changed. Additionally, as a result of the decreasing horizontal velocity component inside the liquid film with increasing depth, the cavity inclines in the direction of the wave propagation, resulting in an asymmetrical expansion of the cavity during the first stages after impingement. The presence or absence of the capillary waves at the left and/or right side of the cavity, in combination with the unequal distribution of the surface tension forces over the cavity surface induces an asymmetrical receding and retraction of the cavity, as well as an inclined Worthington jet.

By varying the phase of the solitary surface wave at impingement, a clear difference in the prompt splash mechanism and the formation of the corona is present. Depending on the wave-phase strong interactions of the expanding corona with the leading or trailing edge of the solitary wave are the result. For relatively low phase angles large cavities with a sharp inclination in the direction of the wave propagation are formed, whereas for relatively high phases the expansion phase of the cavity is influenced only in a minor way. The formation, strength and movement of the capillary waves change magnificently for different phases. For small phases, a single strong capillary wave is formed at the left side of the cavity, for intermediate phases at the right side, and for large phases at both sides of the cavity, but lagged in time between the left and right side of the cavity. These differences lead to completely different recedings and retractions of the cavities and subsequent different Worthington jets.

A higher Weber number of the impinging drop leads to a pronounced prompt splash, a higher, larger and unstable corona and a cavity with a larger maximum diameter and depth. An inclination of the cavity is observed for all Weber numbers, where the angle of inclination increases sharply for larger Weber numbers. For lower Weber numbers an earlier receding and retraction occurs; the receding itself, however, is for all Weber numbers highly asymmetrical, due to the presence of a strong capillary wave at the right side and the absence or presence of a weak capillary wave at the left side of the cavity.

Changing the amplification, i.e. maximum amplitude and propagation velocity, of the solitary surface wave has a distinct effect on the time evolution of the cavity's shape for all investigated wave-phases. A larger amplitude of the wave leads to a strong interaction of the corona with the leading or trailing edge of the surface of the wave and a smaller penetration velocity of the cavity during the expansion phase. During the receding and retraction phases only minor differences are observed between the two waves for relatively large wave-phases, whereas for low wave-phases an earlier and asymmetric receding and retraction is observed for the low amplified wave. The Worthington jet is thicker and reaches a lower maximum height for the high amplified waves, partly due to the strong energy dissipation during the retraction and partly due to the weak surface tension forces acting on the small cavity. A thin, high central jet is observed for the low amplified waves, having a slight inclination as a result of the slight asymmetrical receding and retraction of the cavity.

The last parameter that has been changed, is the value of the viscosity and surface tension of the liquid film and the impinging drop. Large differences in the time evolution of the cavity shape are only observed for small phases of the wave. A lower value of the viscosity leads to a cavity that expands more in radial direction, resulting in larger values of the maximum depth and diameter. Also, the inclination of the cavity increases more rapidly for increasing times after impingement, as a result of the stronger propagation of the top of the cavity in

the direction of the wave propagation, in combination with the decrease of the film velocity for increasing depth.

An earlier and asymmetric receding and retraction of the cavity is seen for a low value of the viscosity, which, in combination with the weak surface tension forces, leads to a thick, short Worthington jet. As a result of the pronounced asymmetrical receding and retraction of the cavity for a higher value of the viscosity, the Worthington jet is highly curved at formation, erecting itself for later time instants.

In the second paragraph of this chapter the results of the single drop impingement measurements and numerical simulations onto the first half part of the wave, $0° \leq \varphi \leq 180°$, have been presented in detail for two classes of surface waves: the standing waves and the solitary surface waves. The presentation of the results was split up into two main parts, each of which focussed on both the depth and the absolute and relative diameter evolution of the cavity in time for the complete impingement process, hence from the first moment of impingement until the central jet is formed after the cavity has retracted. The left and right relative diameter of the cavity were defined as the distances from the vertical axis going through the center of the drop before impingement to the left and right surface of the cavity. Both the absolute and the relative diameter were obtained at the vertical position that equalled half of the maximum depth of the cavity.

The first part focussed on the change of the depth and diameter of the cavity onto a standing surface wave; hence the phase of the wave upon impingement and thus the local inclination of the liquid film could be varied. With these results the influence of the local inclination of the surface film and the local differences of the film height at both sides of the impingement point could be studied. To achieve this goal, fully three-dimensional numerical simulations of the single drop impingement onto a standing wave have been conducted. For these simulations, a surface wave has been initiated, which leveled-off in time due to the influence of surface tension and gravity into a steady liquid film of thickness h. This leveling process, however, took much longer than the drop impingement process itself, due to which the wavy liquid surface still influenced the cavity below the liquid surface at the end of the impingement process.

It was found that the inclination of the liquid surface film upon impingement had a very distinct influence on the time evolution of the shape of the cavity and the typical length and time scales of the impingement process. The drop impinged onto a wave-phase of $\varphi = 180°$, resulting in a thicker rim at the left side of the expanding cavity. At this side the rim remained stable, whereas at the right side an unstable corona was formed.

The penetration of the cavity in depth direction was seen to be independent of the inclination angle of the liquid surface and the Weber number, whereas a clear influence of the inclination was observed for the radial expansion. Because of the declining surface film and the constant penetration of the cavity in depth, a larger surface of the cavity was present at the left side of the cavity, resulting in larger values of the surface tension forces and therefore a faster conversion of the kinetic energy. Although the time evolution of the total diameter of the cavity was not influenced by the inclination angle, the inclination of the standing wave led to lower values of the cavity diameter at the left side of the cavity. This difference between the diameters of the cavity at both sides increased more for lower Weber numbers.

Due to the lower rim at the left side of the cavity and the subsequent earlier merging of the rim with the liquid surface, the capillary wave was formed earlier at this side. During the receding and retraction phase this time difference in capillary wave formation at both sides of the cavity introduced several clear differences between the cavities formed after impingement upon steady liquid films and standing waves. For the results of the impingement onto standing

waves these differences were a lower value of the maximum diameter of the cavity, an asymmetrical downward motion of the capillary waves and receding of the cavity, thereby introducing large differences between the values of the local diameters at both sides of the cavity, an asymmetrical merging of the capillary waves and an off-axis Worthington jet of which its inclination and curvature increased with increasing Weber number.

The second part explained the results of the time evolution of the depth and diameter of the cavity evolution in time upon impingement onto a solitary surface wave. The differences in the cavity evolution for a change in the phase of the wave upon impingement, hence the inclination of the surface film, in the absolute Weber number of the impinging drop, formed by the combination of the terminal velocity of the drop upon impingement and the velocity of the solitary surface wave, in the amplification of the surface wave (velocity and maximum amplitude) and in the liquid properties (viscosity) were described and analysed. With these results not only the influence of the inclination of the surface film was studied, but also the velocity of the liquid film, because this parameter is assumed to play a significant role in understanding the spray impingement process. The results of the depth and diameter evolutions of the cavities in time for the impingement upon solitary surface waves showed several interesting phenomena when comparing the results for different wave-phases, drop impingement Weber numbers, wave amplifications and liquids. In general it was found that the maximum amplitude and the velocity of the surface wave had a pronounced influence on the impingement outcomes. Depending on the amplification of the wave, hence the magnitude of the wave amplitude and wave velocity, different conclusions can be drawn.

For the small amplified wave the penetration velocity of the cavity into the liquid film was found to be constant for all investigated absolute Weber numbers and phases of the wave upon impingement. The inclination of the film surface, and thus the phase of the wave, had a very significant influence on the depth evolution and the absolute and relative diameter evolution in time. For very low ($\varphi \leq 20°$) and very high ($\varphi \geq 150°$) wave-phases no clear influence of the inclination of the wave was found on the impingement process, when comparing the results with the outcomes of the impingement process onto steady liquid films. The inclination of the wave surface was too small and the main wave too far away from the impingement point to have a significant influence on the impingement process. For values of the phase of the wave between $20° \leq \varphi \leq 70°$ a clear interaction of the right side of the expanding rim with the leading edge of the advancing wave occurred. This interaction led to the earlier merging of the rim with the surface film at this side of the cavity, resulting in an asymmetrical formation of the capillary waves and receding of the cavity. The same phenomena were observed for wave-phases between $110° \leq \varphi \leq 150°$, where the left side of the expanding rim interacted with the trailing edge of the receding surface wave. For impingements onto the wave-angles $70° \leq \varphi \leq 110°$ a free corona was formed, leading to an approximately equal time instant at which the capillary waves were formed at both sides of the cavity and a symmetrical receding of the cavity.

Concerning the typical length and time scales of the drop impingement process, it could be concluded that the maximum depths and absolute diameters of the cavities, as well as the non-dimensional time instants at which these maximum depths and absolute diameters were reached, were constant and independent of the phases of the wave at impingement and the liquid properties. For the values of the maximum absolute diameter, a weak dependency on the viscosity of the liquids was found, where it was observed that a higher viscosity resulted in a slightly higher value of the absolute maximum depth. Due to the lower maximum amplitude and velocity of the surface wave for a higher value of the viscosity, the expanding motion of the

cavity had less resistance and a weaker interaction of the expanding rim with the surface film occurred, hence a wider cavity was formed.

For a larger absolute Weber number of the impinging drop the cavity expanded radially in a more amount, leading to larger values of the maximum depths and maximum absolute diameter. For both length scales a linear behaviour was found with the mean Weber number, where it was seen that for the same Weber number the typical length scales were larger for the liquid with the higher viscosity, due to the lower maximum amplitude and velocity of the surface wave. The time at which the maximum depth was reached increased quadratically with an increase of the mean Weber number, whereas a linear behaviour was found between the mean Weber number and the time of maximum absolute diameter. Also for these two time scales it was observed that for the same Weber number the values were larger for the liquid with the higher viscosity.

For the large amplified solitary surface wave the penetration velocity of the cavity into the liquid film depended in a great manner on the phases of the wave for all investigated Weber numbers, although no clear dependency on the wave-phase was found. Just as for the small amplified wave, the inclination of the film surface, and thus the phase of the wave, had a very significant influence on the depth evolution and the absolute and relative diameter evolution in time. The combination of the higher velocity of the solitary surface wave from right to left and the increasing surface tension, acting on the expanding cavity, led to a smaller radial expansion of the right side of the cavity than was observed for the small amplified wave. Together with the additional larger expansion of the left side of the cavity, due to the same direction of the expansion and the propagation of the surface wave, this resulted in stronger differences between the relative diameters for both sides of the cavity and thus a stronger asymmetrical expansion and receding of the cavity.

For very low ($\varphi \leq 20°$) and very high ($\varphi \geq 150°$) wave-phases, a small influence of the inclination of the wave was found on the impingement process, where it was observed that the capillary waves at both sides of the cavity were formed a few non-dimensional time instants apart, due to the weak interaction of the expanding rim with either the leading edge or the trailing edge of the surface wave. For values of the phase of the wave between $20° \leq \varphi \leq 70°$ a very distinct interaction of the right side of the expanding rim with the leading edge of the advancing wave occurred. Together with the increasing inclination of the cavity in time, due to the strong interaction of he cavity with the solitary surface wave, this interaction led to the earlier merging of the rim with the surface film at this side of the cavity, resulting in an asymmetrical formation of the capillary waves and receding of the cavity. The same phenomena were observed for wave-phases between $110° \leq \varphi \leq 150°$, where the left side of the expanding rim interacted strongly with the trailing edge of the receding surface wave. For impingements onto the wave-angles $70° \leq \varphi \leq 110°$ a free corona was formed, leading to a cavity, which was elongated in diameter, but had a small depth.

Concerning the typical length and time scales of the drop impingement process, it was found that the values of the maximum depths and absolute diameters of the cavities did not show any dependency on the phases of the wave at impingement and the liquid properties, whereas the values of the non-dimensional time instants at which these maximum depths and absolute diameters were reached showed a linear increase with increasing wave-phases. The dependency of the values of the maximum absolute diameter on the viscosity of the liquids, found for the impingement upon small solitary waves, had disappeared for the large amplified wave.

For a larger absolute Weber number of the impinging drop the cavity expanded radially in a more amount, leading to larger values of the maximum depths, but approximately constant

values of the maximum absolute diameter. The time at which the maximum depth was reached increased quadratically with an increase of the mean Weber number, whereas a linear behaviour was found between the mean Weber number and the time of maximum absolute diameter. The values of both length and time scales did not depend on the liquid properties, meaning that for large amplified waves, hence with a large propagation velocity and maximum amplitude, the viscosity does not play a role anymore in the impingement process. Due to the same surface tensions of both liquids, it could be concluded that for these surface waves the typical time and length scales are a function of the terminal velocity of the drop upon impingement.

A comparison of the results between both solitary surface waves led to the conclusions that due to the higher propagation velocity and higher amplitude of the larger surface wave, a very significant difference between both relative diameters occurred, together with a stronger interaction of the expanding rim with the leading or trailing edge of the surface wave. This led to a cavity that had a smaller maximum depth and absolute diameter, although the typical time scales remained approximately the same.

In general it can therefore be concluded that the waviness, hence inclination, of the surface film, as well as the velocity and amplitude of the surface waves, have a highly significant influence on the single drop impingement results, in particular on the splash mechanism, the corona formation, the evolution of the cavity below the liquid surface and the typical time and length scales of the impingement process. This means that the existing theoretical models, used for the modeling of spray impingement, should definitely be changed by taking into account the significant influences of the film topology on the impingement process.

Part II: Spray impingement

Chapter 6

Experimental setup and measurement techniques

This chapter describes the experimental arrangement designed to investigate the spray impingement process. In order to receive the required data associated with these processes, several optical measurement techniques have been used. These are the *Shadowgraph technique*, *phase-Doppler anemometry* (*PDA*) and *particle image velocimetry* (*PIV*).

The easiest way to visualise the different spray configurations, like the shape of the spray cone, is by using the *Shadowgraph technique*, which uses a high-speed camera in combination with a continuous light source. For spray investigations, it is important to characterise the spray by measuring the droplet size and velocity distribution at different points in space. This is usually done by means of the *phase-Doppler anemometry* technique, a point measurement technique making use of the principle of laser light interference. To measure the velocity distribution and its fluctuations at different depths and positions inside the surface film during spray impingement, two measurement techniques can be applied, *laser-Doppler anemometry* (*LDA*) and *particle image velocimetry* (*PIV*). The first measurement technique is, just like *PDA*, based on the principle of laser light interference. The spatial resolution of this technique is very good, but the main drawback is that it can measure the velocity only in one single point at the time. To measure the film velocity distribution at several positions of a certain two-dimensional plane inside the surface film, all the grid points on this plane have to be measured. This makes this technique very time-consuming, and no instantaneous two-dimensional velocity fields can be determined. To overcome these problems, *PIV*-measurements have been conducted, with which instantaneous velocity fields can be measured directly. The working principles, together with their adaptations to the measurement setup, will be described in detail in §(3.2) for the *Shadowgraph technique* and in §(6.2.1) and §(6.2.2) for the *PDA*-technique and *PIV*-technique respectively.

6.1 Spray impingement layout and operating conditions

The general layout for the spray impingement studies is shown in Figure 6.1. For all investigations presented hereafter, the spray impinges onto the wavy liquid film under atmospheric conditions. An air supply system together with a pressurised reservoir of 45 L (Stracka Bruno GmbH) is used to set an overpressure of 1.54 bar on the liquid supply system. With the use of a volume flow regulator (Cole Parmer, having a flow rate of 40 - 400 mL/min), a variable liquid volume flow can be set for the ultrasonic atomizers (Lechler GmbH). The height of the

atomizers above the surface can be changed with the use of a micrometer traversing system to investigate the influence of the kinetic energy of the impinging drops on the motion of the surface film. The ultrasonic atomizers are operated with and without carrier gas, due to which an extra air supply system is needed. In case of measurements with air as a carrier gas, a constant air overpressure of 0.6 bar is set, whereas for the studies without the carrier gas the atmospheric air pressure is used.

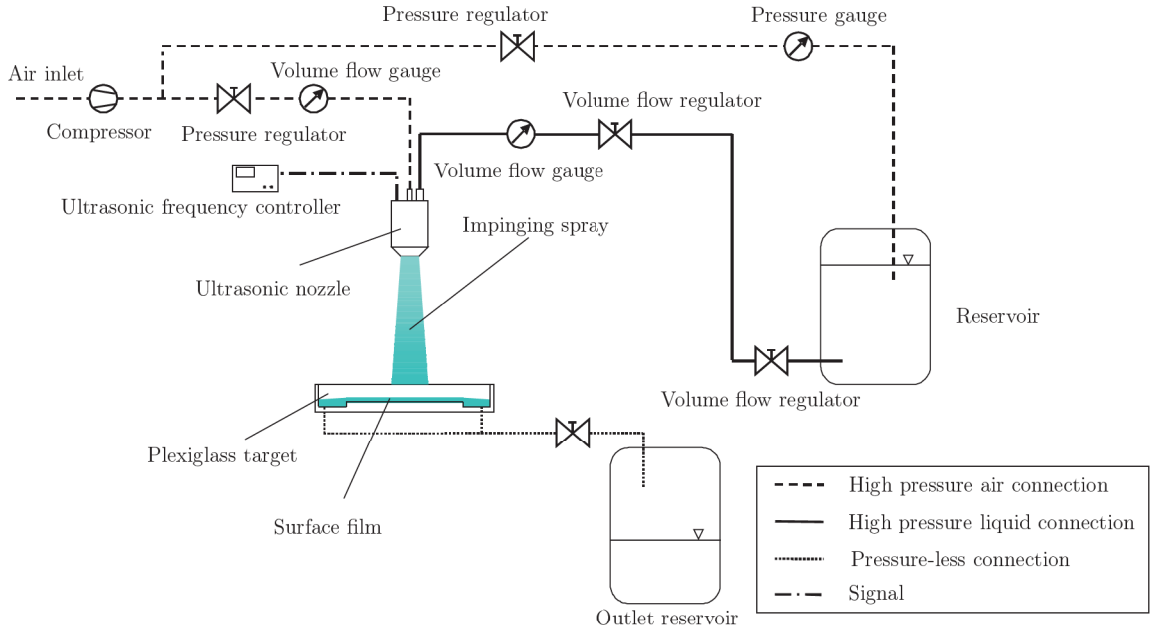

Figure 6.1: Experimental arrangement for spray impingement on a highly unsteady, wavy surface film

The investigated spray impinges onto a circular Plexiglass plate with a diameter of 200 mm. Plexiglass is taken to assure a good optical access to the wavy surface film for the PIV-measurements from below, §(6.2.2). This inner Plexiglass plate lies 5 mm higher than the Plexiglass container of 300 mm in diameter, in order to allow the liquid film, continuously built up on the inner Plexiglass plate due to the constant spray volume flow, to flow off the impingement plate. In this way a constant film thickness is achieved. After impingement, the liquid is collected into an outlet reservoir, to be reused when the pressurised reservoir is empty.

For the spray impingement investigations two different ultrasonic atomizers are used, US10 and US20, having a volume flow range of 1 - 10 L/h and 2 - 20 L/h respectively. The designs of the atomizers are given in Figure 6.2.

The atomizers make use of piezoceramic elements in order to generate mechanical oscillations from electric waves. After amplification, these mechanical oscillations are transmitted to the atomizer. A thin liquid film is obtained by means of a uniform distribution of the liquid on the atomizer's surface. By means of the mechanical oscillations by the vibrating plate capillary waves are produced on the film surface, which become instable and fine drops are detached off the liquid surface. These drops exit the atomizer with parabolically shaped trajectories. To obtain the best atomization for each liquid having different viscosities and surface tensions, an optimum high-frequency power can be set at the controller. By doing so, a relatively narrow

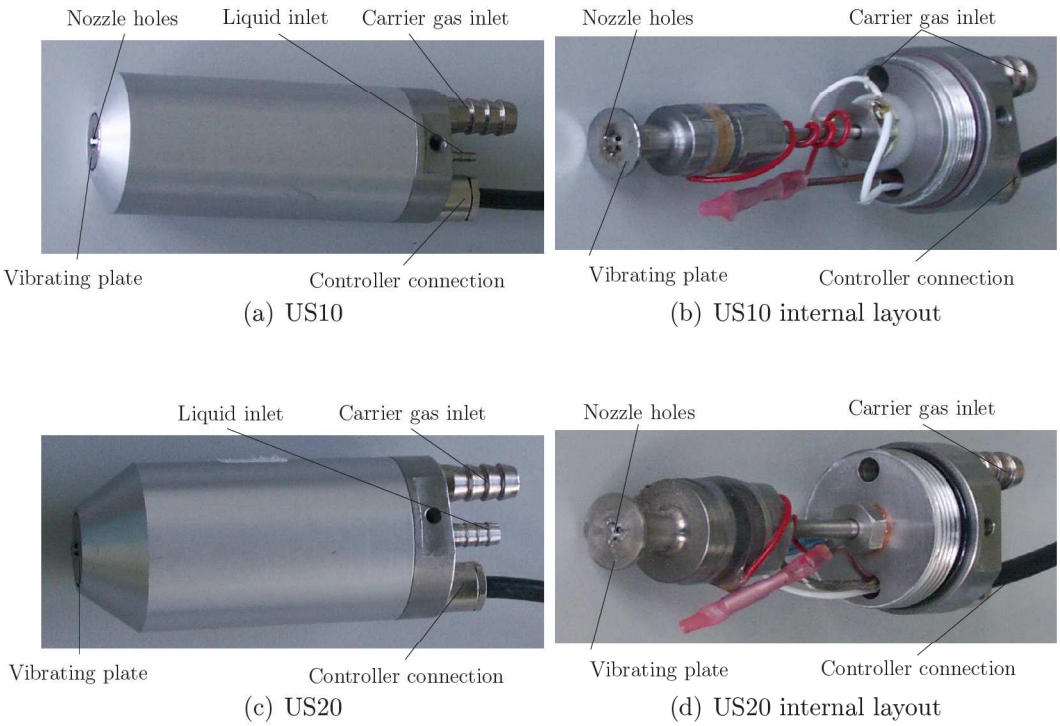

(a) US10 (b) US10 internal layout

(c) US20 (d) US20 internal layout

Figure 6.2: Ultrasonic atomizers US10 and US20

Table 6.1: Operating conditions for spray impingement

	Atomizer	
	US10	**US20**
Liquid	Water/Glycerine (70%/30%)	Water/Glycerine (70%/30%)
Density ρ $[kg/m^3]$	1179	1179
Viscosity μ $[kg/(m \cdot s)]$	$2.3 \cdot 10^{-3}$	$2.3 \cdot 10^{-3}$
Surface tension σ $[kg/s^2]$	$2.36 \cdot 10^{-2}$	$2.36 \cdot 10^{-2}$
Volume flow $[mL/min]$	50, 100, 150 and 200	100, 200, 300 and 400
Liquid overpressure $[bar]$	1.540	1.540
Carrier gas	With/without air	With/without air
Carrier gas overpressure $[bar]$	0.604	0.604
Impingement height $[mm]$	48.8 and 110	61.3 and 122.5

drop spectrum with a distinct maximum can be obtained.

The measurement conditions for the spray impingement studies are given in Table 6.1. For all the investigations, a mixture of glycerine and distilled water (30%Vol to 70%Vol) is used at atmospheric conditions. For each atomizer four different volume flows have been chosen to obtain the influence of this parameter on the drop diameters and drop velocities before impingement, as well as on the surface film radial velocity distributions after impingement. The liquid overpressure is held constant at 1.54 bar. The influence of the carrier gas is also obtained, as the measurements are conducted with and without air. With the air supply, the air overpressure is set at 0.604 bar, whereas without the use of the carrier gas, the atmospheric gas pressure is used. Furthermore, for each atomizer, two different impingement heights are studied, for US10 48.8 mm and 110 mm, and 61.3 mm and 122.5 mm for US20.

6.2 Principles, data processing and adaptations of the measurement techniques used

Table 6.2 gives an overview of the applied measurement techniques and the goals (i.e. obtained parameters) of these techniques. The applied techniques are all standard measurement techniques, described very well in literature. In the detailed survey for each measurement technique given below, only a short overview of the working principle of each technique will therefore be given, as well as the adaptation of every technique to the aims of the study of the impingement processes and the analysis of the recorded data. The principle of the shadowgraphy technique has already been explained in Chapter 3.

Table 6.2: Overview of different applied measurement techniques

Technique	**Goal**	**Comments**
Phase-Doppler Anemometry (*PDA*)	Measurement of drop diameter and drop velocity	Many drops required, high spatial resolution possible, point measurement technique
Particle Image Velocimetry (*PIV*)	Measurement of film velocity distribution	Measurement using tracer particles, planar or volumetric technique, high spatial and temporal resolution possible, time-resolved

6.2.1 Phase-Doppler anemometry

Working principle

The *phase-Doppler anemometry*-technique is an optical measurement technique to determine up to three velocity components, in combination with the diameter of spherical and non-spherical particles and drops. The working principle of this technique is explained in detail in literature, for example in Albrecht *et al.* [1] and Ruck [141]. Therefore, only a brief explanation of this technique will be given here.